

Low-lying Odd-parity States of the Nucleon in Lattice QCD

M. Selim Mahbub,¹ Waseem Kamleh,¹ Derek B. Leinweber,¹ Peter J. Moran,¹ and Anthony G. Williams¹
(CSSM Lattice Collaboration)

¹*Special Research Centre for the Subatomic Structure of Matter,
School of Chemistry & Physics, University of Adelaide, SA 5005, Australia*

The world's first examination of the odd-parity nucleon spectrum at light quark masses in $2 + 1$ flavor lattice QCD is presented. Configurations generated by the PACS-CS collaboration and made available through the ILDG are used, with the lightest pion mass at 156 MeV. A novel method for tracking the individual energy eigenstates as the quark mass changes is introduced. The success of this approach reveals the flow of the states towards the physical masses. Using the correlation matrix method, the two lowest-energy states revealed are found to be in accord with the physical spectrum of Nature.

PACS numbers: 11.15.Ha,12.38.Gc,12.38.-t

Lattice QCD is the only currently known *ab-initio* or first-principles approach to the fundamental quantum field theory governing the properties of hadrons, Quantum Chromodynamics (QCD). While the ground-state hadron spectrum of QCD is well understood, a determination of the excited state energy spectrum is in the process of being revealed. Ultimately, the results can be compared with the existing experimental data and provide predictions and motivations for future experiments.

Hadron spectroscopy is dependent on the rich dynamics of the strong interaction. For example, the experimentally observed mass of the first positive-parity excitation of the nucleon, known as the Roper resonance, $N_{\frac{1}{2}}^{+}(1440) P_{11}$, is surprising low compared to the lowest-lying negative-parity partner, $N_{\frac{1}{2}}^{-}(1535) S_{11}$. This phenomenon is not observed in constituent or valence quark models where the lowest-lying odd-parity state occurs naturally *below* the first $J^P = \frac{1}{2}^{+}$ excitation.

Drawing on experimental results, we note that the Breit-Wigner width of the $N^{-}(1535)$ state is ≈ 150 MeV, approximately half the width of the Roper $N^{+}(1440)$ [1]. Furthermore, the branching fraction $\Gamma(\pi N)/\Gamma$ for $N^{-}(1535)$ is $2/3$ of the Roper. Together, these factors indicate a suppression of $1/3$ in the coupling of πN to the $N^{-}(1535)$ state relative to the Roper. Noting that the light πN dressing makes the most important self-energy contribution, it is anticipated that the self-energy dressings of πN for the $N^{-}(1535)$ will be reduced to approximately 10% of that for the Roper. A consequence of this is to suppress the finite-volume effects of the lattice QCD simulation which can otherwise lead to large energy shifts associated with the avoidance of energy-level crossings of the single and multi-particle scattering states. Similar arguments for the $N^{-}(1650)$ suggest πN self-energy contributions are suppressed to the 25% level. Thus, it is interesting to directly compare the results of our lattice QCD simulations with experiment and gain insight on the quark mass dependence of these states. While finite-volume effects are of resid-

ual interest in this investigation, understanding the finite volume effects on these states and linking them to the resonances of Nature is a long term program of the lattice QCD community.

The experimentally observed nearly-degenerate $S_{11}(1535)$ and (1650) states are in agreement with the simple quark-model predictions based on $SU(6)$ symmetry. Therefore, looking at the low-lying $N_{\frac{1}{2}}^{-}$ energy states and their structure from the first principles approach is potentially very revealing. Some recent full QCD results can be seen in Refs. [2–7]. Herein, it will be interesting to explore the physics associated with the dynamical fermion loops of full QCD, this time at very light quark masses.

The correlation functions for the $N_{\frac{1}{2}}^{-}$ states are short-lived compared to the lighter $N_{\frac{1}{2}}^{+}$ ground state. Thus it is important to adopt a method that can isolate the effective-mass plateaus at early Euclidean times. The variational method [8, 9] is the state-of-the-art approach for achieving this in lattice hadron-spectroscopy calculations and is adopted here. Through a generalized eigenvalue analysis of a matrix of correlation functions, the process enables one to create highly optimized interpolating fields designed to excite a single energy eigenstate of the QCD Hamiltonian. The masses of the energy states are then obtained through a standard effective-mass analysis [10] providing a robust approach for extracting the energy states at early Euclidean times.

In this paper, we utilize the established approach of Refs. [6, 7] to explore the low-lying $N_{\frac{1}{2}}^{-}$ energy states in full QCD. In doing so, a novel method has been developed to track the energy eigenstates from heavy to light quark masses. The method is particularly useful when the energy-states are nearly degenerate.

The two-point correlation-function matrix for $\vec{p} = 0$

can be written as

$$G_{ij}^{\pm}(t) = \sum_{\bar{x}} \text{Tr}_{\text{sp}} \{ \Gamma_{\pm} \langle \Omega | \chi_i(x) \bar{\chi}_j(0) | \Omega \rangle \}, \quad (1)$$

$$= \sum_{\alpha} \lambda_i^{\alpha} \bar{\lambda}_j^{\alpha} e^{-m_{\alpha} t}, \quad (2)$$

where Dirac indices are implicit, λ_i^{α} and $\bar{\lambda}_j^{\alpha}$ are the couplings of interpolators χ_i and $\bar{\chi}_j$ at the sink and source respectively, α enumerates the energy eigenstates with mass m_{α} , and $\Gamma_{\pm} = (\gamma_0 \pm 1)/2$ projects the parity of the eigenstates. A linear superposition of interpolators $\bar{\phi}^{\alpha} = \sum_j \bar{\chi}_j u_j^{\alpha}$ creating state α provides the relationship

$$G_{ij}(t_0 + \Delta t) u_j^{\alpha} = e^{-m_{\alpha} \Delta t} G_{ij}(t_0) u_j^{\alpha}, \quad (3)$$

from which right and left eigenvalue equations are obtained

$$[(G(t_0))^{-1} G(t_0 + \Delta t)]_{ij} u_j^{\alpha} = c^{\alpha} u_i^{\alpha}, \quad (4)$$

$$v_i^{\alpha} [G(t_0 + \Delta t) (G(t_0))^{-1}]_{ij} = c^{\alpha} v_j^{\alpha}, \quad (5)$$

with $c^{\alpha} = e^{-m_{\alpha} \Delta t}$. The vectors u_j^{α} and v_i^{α} diagonalize the correlation matrix at time t_0 and $t_0 + \Delta t$ making the projected correlation matrix, $v_i^{\alpha} G_{ij}^{\pm}(t) u_j^{\beta} \propto \delta^{\alpha\beta}$. The parity and eigenstate projected correlator,

$$G_{\pm}^{\alpha} \equiv v_i^{\alpha} G_{ij}^{\pm}(t) u_j^{\alpha}, \quad (6)$$

is then analyzed to obtain masses of energy-states.

A eigenvector analysis of a symmetric matrix having orthogonal eigenvectors can be constructed by inserting $G(t_0)^{-\frac{1}{2}} G(t_0)^{\frac{1}{2}} = I$, in Eq. (4) and multiplying by $G(t_0)^{\frac{1}{2}}$ from the left,

$$G(t_0)^{-\frac{1}{2}} G(t_0 + \Delta t) G(t_0)^{-\frac{1}{2}} G(t_0)^{\frac{1}{2}} u^{\alpha} = c^{\alpha} G(t_0)^{\frac{1}{2}} u^{\alpha}, \quad (7)$$

$$G(t_0)^{-\frac{1}{2}} G(t_0 + \Delta t) G(t_0)^{-\frac{1}{2}} w^{\alpha} = c^{\alpha} w^{\alpha}, \quad (8)$$

where, $w^{\alpha} = G(t_0)^{\frac{1}{2}} u^{\alpha}$ and $[G(t_0)^{-\frac{1}{2}} G(t_0 + \Delta t) G(t_0)^{-\frac{1}{2}}]$ is a real symmetric matrix, with orthogonal eigenvectors w^{α} . The vector u^{α} may be recovered from the w^{α} via $u^{\alpha} = G(t_0)^{-\frac{1}{2}} w^{\alpha}$.

The PACS-CS 2 + 1 flavor dynamical-fermion configurations [11] made available through the ILDG [12] are used herein. These configurations use the non-perturbatively $\mathcal{O}(a)$ -improved Wilson fermion action and the Iwasaki-gauge action [13]. The lattice volume is $32^3 \times 64$, with $\beta = 1.90$ providing a lattice spacing of $a = 0.0907$ fm and a physical volume of $\approx (2.90 \text{ fm})^3$. Five values of the (degenerate) up and down quark masses are considered, with hopping parameter values of $\kappa_{ud} = 0.13700, 0.13727, 0.13754, 0.13770$ and 0.13781 , corresponding to pion masses of $m_{\pi} = 0.702, 0.572, 0.413, 0.293, 0.156$ GeV [11]; for the strange quark

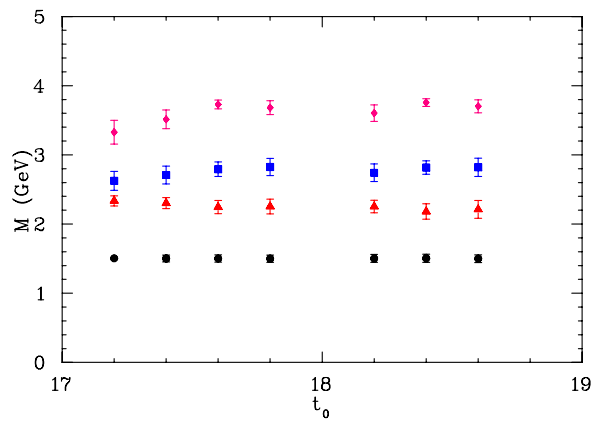


FIG. 1. (Color online). $N_{\frac{1}{2}}^{-}$ energy-states from a 4×4 correlation matrix analysis of the χ_1 interpolator at the lightest pion mass of $m_{\pi} = 156$ MeV. The variational parameters t_0 and Δt are shown at the major and minor tick marks respectively. The LHS of the diagram refers to $t_0 = 17$, while the RHS is for $t_0 = 18$.

$\kappa_s = 0.13640$. Gauge-invariant Gaussian smearing [14] is used at the fermion source and sink with a fixed smearing fraction and four different smearing levels including 16, 35, 100, and 200 sweeps [6, 7].

The complete set of local interpolating fields with three different spin-flavor combinations for the spin- $\frac{1}{2}$ nucleon are considered herein,

$$\chi_1(x) = \epsilon^{abc} (u^{Ta}(x) C \gamma_5 d^b(x)) u^c(x), \quad (9)$$

$$\chi_2(x) = \epsilon^{abc} (u^{Ta}(x) C d^b(x)) \gamma_5 u^c(x), \quad (10)$$

$$\chi_4(x) = \epsilon^{abc} (u^{Ta}(x) C \gamma_5 \gamma_4 d^b(x)) u^c(x). \quad (11)$$

Each interpolator has a unique Dirac structure giving rise to different spin-flavor combinations. Moreover, as each spinor has upper and lower components, with the lower components containing an implicit derivative, different combinations of zero, one and two-derivative interpolators are provided. The interpolator χ_4 is the time component of the local spin- $\frac{3}{2}$ isospin- $\frac{1}{2}$ interpolator which also couples to spin- $\frac{1}{2}$ states. It provides a different linear combination of zero- and two-derivative terms complementary to χ_1 .

In Fig. 1, projected masses of the $N_{\frac{1}{2}}^{-}$ states are presented from a 4×4 correlation matrix constructed from the interpolator χ_1 and four different smearing levels. The dependence of the results on the variational parameters t_0 and Δt is illustrated. While the lowest energy-state is almost independent of t_0 and Δt , the excited states show some dependence at smaller t_0 and Δt values. The energy-states at $(t_0, \Delta t) = (18, 2)$ provide the best balance between the systematic and statistical uncertainties [6] and these parameters are therefore selected for our numerical study.

In Fig. 2 we show results for the lowest energy-state from dynamical and quenched [15] QCD simulations. As

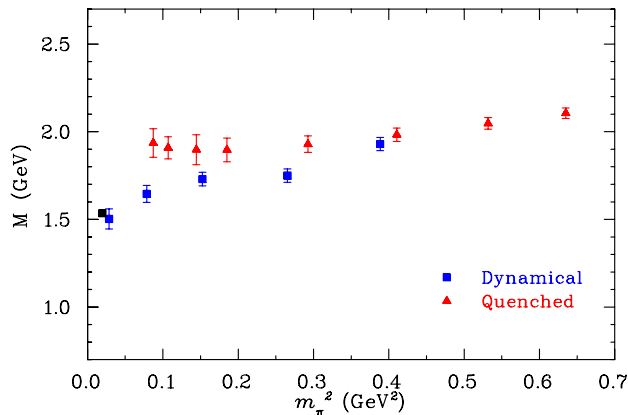


FIG. 2. (Color online). Dynamical and quenched results for the lowest $N\frac{1}{2}^-$ energy-state using the χ_1 interpolator.

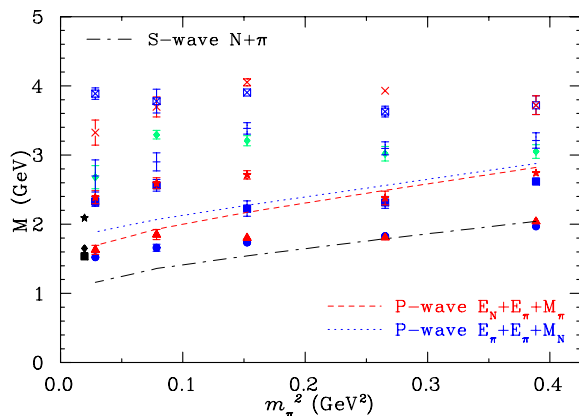


FIG. 3. (Color online). $N\frac{1}{2}^-$ energy-states from an 8×8 correlation matrix of χ_1 and χ_2 interpolators, for the pion mass range of 156 to 702 MeV. The physical $N\frac{1}{2}^-$ spectrum [1] is shown at the far left.

anticipated, the quenched and dynamical results are in agreement in the heavy quark-mass region. However, in the light quark-mass regime the results are significantly different as the effects of the light sea quarks become increasingly important. Only the dynamical results approach the physical value and this provides strong evidence for the non-trivial role of light sea-quark degrees of freedom to the structure of Nature's hadron spectrum.

To explore the nearby second energy state, S_{11} (1650), we extend our analysis to include the interpolators χ_2 and χ_4 with a variety of smearing levels. The results of an 8×8 correlation-matrix analysis of χ_1 and χ_2 interpolators with four levels of smearing are presented in Fig. 3.

The flow of the lowest two energy states towards the physical values is remarkable. The results at the two heaviest pion masses sit close to the scattering S-wave $N+\pi$ threshold indicating that the results for these heaviest pion masses may be scattering states. However, in the light quark-mass region these states move above the threshold.

It is likely that the three-quark interpolators used herein have relatively small couplings to the scattering states at the light quark masses relative to the states observed and are not resolved in the correlation-matrix analysis. Hence, a combination of five- and three-quark interpolators in a correlation matrix analysis is highly desirable for future investigations to ensure better overlap with the multi-particle states. This type of novel work using the stochastic LapH method is in progress [16]. It is because the coupling to multi-particle states at light quark masses is heavily suppressed, that it is meaningful to compare lattice results with the central values of experimentally measured hadron resonances.

A similar situation prevails for the second pair of states in the spectrum, where the states sit close to the P -wave $E_N + E_\pi + M_\pi$ and $E_\pi + E_\pi + M_N$ threshold scattering states with back-to-back momenta of one lattice unit, $\vec{p} = (2\pi/L_x, 0, 0)$. The apparent flow of these states in the light-quark region toward the physical S_{11} (2090) state is also interesting.

In presenting the results of Fig. 3 and assigning symbols to each of the energy levels observed at a particular quark mass, it is necessary to track the evolution of the states from one quark mass to the next. We have done this through a consideration of the evolution of the eigenvectors as the quark mass is changed.

Consider M interpolating fields making an $M \times M$ parity-projected correlation matrix $G(t)$ and its associated symmetric generalized eigenvalue equation of Eq. (8). Using the normalization $\sum_i^M |w_i^\alpha|^2 = 1$, the quantity $\vec{w}^\alpha(m_q) \cdot \vec{w}^\beta(m_{q'}) = \delta_{\alpha\beta}$. This feature enables the use of the generalized measure

$$\mathcal{W}^{\alpha\beta}(m_q, m_{q'}) = \vec{w}^\alpha(m_q) \cdot \vec{w}^\beta(m_{q'}) \quad (12)$$

to identify the states most closely related as we move from quark mass m_q to an adjacent quark mass $m_{q'}$. The state numbers α and β are assigned in order of increasing projected eigenstate energy at the quark masses m_q and $m_{q'}$ respectively. Typical results for this generalized measure of eigenvector overlap are presented in Table I.

For each value of state index α there is only one value of β where the magnitude of the entry is significantly larger than all others and approaching unity. The most relevant entries for consideration are the immediate neighbors of α where a crossing of the eigenvectors moves the largest entry off the diagonal.

This measure provides a clear identification of how states in the spectrum at quark mass m_q are associated with states at the next value of quark mass, $m_{q'}$. For example, the results of Table I indicate the first four states at $m_{q'}$ appear with the same ordering in the spectrum as observed at m_q , the fifth state at $m_{q'}$ is associated with the sixth state at m_q and vice versa and similarly for the seventh and eighth states. We note that while the central values of the energies have changed order, the error bars are sufficiently large that one cannot conclude that an

TABLE I. The scalar product $\vec{w}^\alpha(m_q) \cdot \vec{w}^\beta(m_{q'})$ for $\kappa = 0.13754$ ($m_\pi = 413$ MeV) and $\kappa' = 0.13770$ ($m_\pi = 293$ MeV) for an 8×8 correlation matrix of χ_1 and χ_2 with four different levels of smearing. State numbers α and β correspond to row and column number, respectively.

0.91	0.40	0.02	0.02	0.01	-0.05	0.00	0.00
0.40	-0.91	0.00	0.01	-0.02	0.01	-0.01	0.00
-0.01	-0.01	0.96	-0.27	0.01	-0.01	0.00	0.02
-0.03	0.00	0.27	0.96	0.01	0.01	0.02	0.00
0.04	0.03	0.01	-0.01	-0.22	0.97	0.02	0.01
0.01	-0.01	-0.01	-0.01	0.98	0.22	0.04	0.00
0.00	0.00	-0.02	0.01	0.01	-0.01	-0.12	0.99
0.01	-0.01	0.00	-0.02	-0.04	-0.03	0.99	0.12

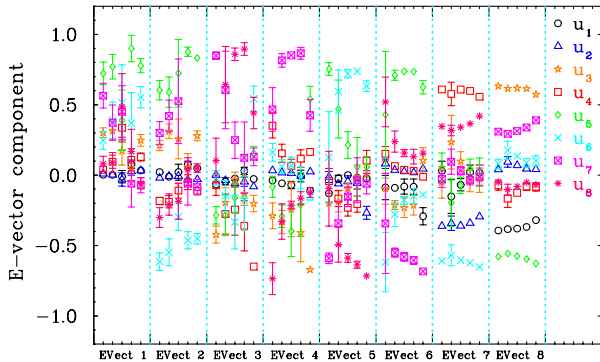


FIG. 4. (Color online). The components of the eigenvector u^α providing the amplitude for each interpolating field at the source for creating the state α . The states are labeled by the eigenvector (EVect) number with the ordering as provided in Fig. 3 at the heaviest quark mass. For each EVect, the eigenvector components are plotted from left to right in order of increasing quark mass. In the legend, (u_1, u_2) , (u_3, u_4) , (u_5, u_6) and (u_7, u_8) correspond to the smearing-sweep levels of 16, 35, 100 and 200 respectively. Odd numbers in the subscripts correspond to the contribution from the χ_1 interpolator, whereas, even numbers correspond to χ_2 .

avoided energy level crossing has taken place in moving from quark mass m_q to $m_{q'}$.

The components of the eigenvector u^α , providing the amplitude for each interpolating field at the source for creating the state α , are provided in Fig. 4. A non-trivial contribution from both the χ_1 and χ_2 interpolators for the lowest two energy-states is evident. The scalar-diquark interpolator χ_1 dominates the lowest energy-state. On the other hand, both χ_1 and χ_2 interpolators have large contributions to the second energy state where their strengths appear with opposite signs. The eigenvector components typically display a slow evolution as the quark mass is changed.

The energy-states for our complete analysis are presented in Fig. 5. The results are drawn from two 8×8 correlation-matrix analyses for pairs of χ_1, χ_2 and χ_1, χ_4 . The matrices are formed with each interpolator having four levels of smearing. Whereas the χ_1, χ_2 and χ_2, χ_4 analyses reveal a similar spectrum, four new states are

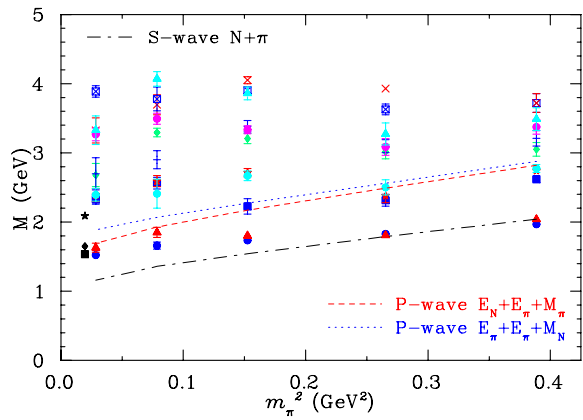


FIG. 5. (Color online). Masses of 12 low-lying $N\frac{1}{2}^-$ energy states from two 8×8 correlation matrices of χ_1, χ_2 and χ_1, χ_4 .

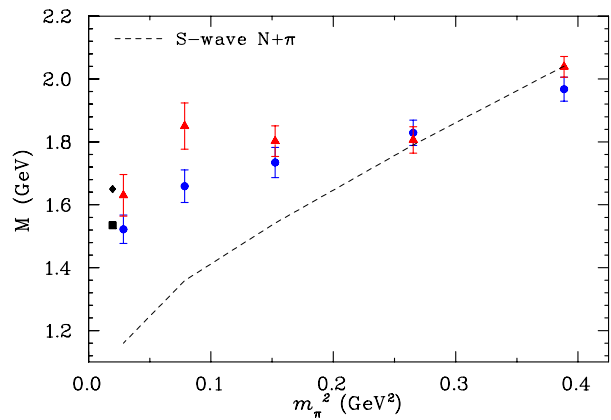


FIG. 6. (Color online). The quark mass dependence of the lowest two lowest-lying $N\frac{1}{2}^-$ states are compared with the S -wave scattering threshold.

revealed in the χ_1, χ_4 analysis providing the resolution of 12 low-lying states in our analysis.

In the quark model based on $SU(6)$ spin-flavor symmetry, the odd parity (1535) and (1650) states belong to the negative parity, $L = 1$, 70-plet representation of $SU(6)$. As three spin- $\frac{1}{2}$ quarks may combine to a total spin of $s = \frac{1}{2}$ or $\frac{3}{2}$, the $L = 1$ state can couple two different ways to provide a $J = \frac{1}{2}$ state, hence providing two orthogonal spin- $\frac{1}{2}$ states in the $L = 1$, 70-plet representation. Both of these states have a width of ≈ 150 MeV. The lowest two energy states revealed here are similarly close in mass, as illustrated in Fig. 5, in accord with the $SU(6)$ quark model.

These two lowest-lying $N\frac{1}{2}^-$ states are presented in Fig. 6 in comparison with the S -wave scattering threshold. These lattice results, providing the first examination of the odd-parity nucleon spectrum at a pion mass as low as 156 MeV, display remarkable agreement with the physical values. They represent a significant achievement for lattice regularized QCD in describing Nature.

Although both these low-lying states are quite similar

at the two heaviest quark masses, their approach to the physical values in the light quark-mass region are different. Significant chiral curvature is evident, in particular for the second state. It will be interesting to explore the mass dependence of these states using effective field theory techniques and to repeat these studies on matched lattices of different volume when they become available. Future studies will endeavor to observe the multi-particle scattering states and determine the resonance parameters of these states from the first principles of QCD.

This research was undertaken on the NCI National Facility in Canberra, Australia, which is supported by the Australian Commonwealth Government. We also acknowledge eResearch SA for generous grants of super-computing time. This research is supported by the Australian Research Council.

[1] K. Nakamura *et al.* (Particle Data Group), *J. Phys.*, **G37**, 075021 (2010).
 [2] J. M. Bulava *et al.*, *Phys. Rev.*, **D79**, 034505 (2009), arXiv:0901.0027 [hep-lat].
 [3] J. Bulava *et al.*, *Phys. Rev.*, **D82**, 014507 (2010), arXiv:1004.5072 [hep-lat].

[4] G. P. Engel, C. B. Lang, M. Limmer, D. Mohler, and A. Schafer (BGR [Bern-Graz-Regensburg]), *Phys. Rev.*, **D82**, 034505 (2010), arXiv:1005.1748 [hep-lat].
 [5] R. G. Edwards, J. J. Dudek, D. G. Richards, and S. J. Wallace, *Phys. Rev.*, **D84**, 074508 (2011), arXiv:1104.5152 [hep-ph].
 [6] M. S. Mahbub, W. Kamleh, D. B. Leinweber, P. J. Moran, and A. G. Williams (CSSM Lattice), *Phys. Lett.*, **B707**, 389 (2012), arXiv:1011.5724 [hep-lat].
 [7] B. J. Menadue, W. Kamleh, D. B. Leinweber, and M. S. Mahbub, *Phys. Rev. Lett.*, **108**, 112001 (2012), arXiv:1109.6716 [hep-lat].
 [8] C. Michael, *Nucl. Phys.*, **B259**, 58 (1985).
 [9] M. Luscher and U. Wolff, *Nucl. Phys.*, **B339**, 222 (1990).
 [10] M. S. Mahbub *et al.*, *Phys. Lett.*, **B679**, 418 (2009), arXiv:0906.5433 [hep-lat].
 [11] S. Aoki *et al.* (PACS-CS), *Phys. Rev. D*, **79**, 034503 (2009), arXiv:0807.1661 [hep-lat].
 [12] M. G. Beckett *et al.*, *Comput. Phys. Commun.*, **182**, 1208 (2011), arXiv:0910.1692 [hep-lat].
 [13] Y. Iwasaki, (1983), uTHEP-118.
 [14] S. Gusken, *Nucl. Phys. Proc. Suppl.*, **17**, 361 (1990).
 [15] M. S. Mahbub, W. Kamleh, D. B. Leinweber, A. O. Cais, and A. G. Williams, *Phys. Lett.*, **B693**, 351 (2010), arXiv:1007.4871 [hep-lat].
 [16] C. Morningstar *et al.*, *Phys. Rev.*, **D83**, 114505 (2011), arXiv:1104.3870 [hep-lat].